

# Testing isotropy in the Universe using photometric and spectroscopic data from the SDSS

Suman Sarkar<sup>1</sup><sup>★</sup>, Biswajit Pandey<sup>1</sup><sup>†</sup> and Rishi Khatri<sup>2</sup><sup>‡</sup>

<sup>1</sup> Department of Physics, Visva-Bharati University, Santiniketan, Birbhum, 731235, India

<sup>2</sup> Department of Theoretical Physics, Tata Institute of Fundamental Research, Mumbai, 400005, India

29 July 2021

## ABSTRACT

We analyze two volume limited galaxy samples from the SDSS photometric and spectroscopic data to test the isotropy in the local Universe. We use information entropy to quantify the global anisotropy in the galaxy distribution at different length scales and find that the galaxy distribution is highly anisotropic on small scales. The observed anisotropy diminishes with increasing length scales and nearly plateaus out beyond a length scale of  $200h^{-1}\text{Mpc}$  in both the datasets. We compare these anisotropies with those predicted by the mock catalogues from the N-body simulations of the  $\Lambda\text{CDM}$  model and find a fairly good agreement with the observations. We find a small residual anisotropy on large scales which decays in a way that is consistent with the linear perturbation theory. The slopes of the observed anisotropy converge to the slopes predicted by the linear theory beyond a length scale of  $\sim 200h^{-1}\text{Mpc}$  indicating a transition to isotropy. We separately compare the anisotropies observed across the different parts of the sky and find no evidence for a preferred direction in the galaxy distribution.

**Key words:** methods: numerical - galaxies: statistics - cosmology: theory - large scale structure of the Universe.

## 1 INTRODUCTION

The statistical homogeneity and isotropy of the Universe is a fundamental premise of modern cosmology. The assumption of homogeneity and isotropy of the Universe is known as the Cosmological principle. The isotropy of the Universe demands that at any given instant of time, there are no special directions in the Universe. This assumption, considered to be a cornerstone of the standard cosmological model, can be tested with the plethora of data from the modern cosmological observations. The discovery of the Cosmic Microwave Background radiation (CMB) in 1964 (Penzias & Wilson 1965) proved to be a milestone in the establishment of the standard model of cosmology. The Cosmic Background Explorer (COBE) mission launched in 1990 revealed the uniformity of the CMB temperature across the entire sky (Smoot et al. 1992; Fixsen et al. 1996) and provided one of the most powerful evidences in favour of isotropy. COBE and two subsequent space missions, Wilkinson Microwave Anisotropy Probe (WMAP) and Planck, along with numerous ground and balloon based experiments (Komatsu et al. 2011; Planck Collaboration et al. 2016a; Crill et al.

2003; Fowler et al. 2007; Carlstrom et al. 2011) measured the small anisotropies in the CMB sky revealing a wealth of cosmological information and ushering in the era of precision cosmology. The CMB anisotropies are small fluctuations in the CMB temperature or intensity as a function of position on the sky.

We should clarify here that even though there are small anisotropies in the CMB, we can still have *statistical isotropy*. Statistical isotropy implies that the small fluctuations in the CMB should look same in every direction in the sky. In other words, the angular power spectrum of anisotropies should not depend on which part of the sky we choose to study. Even on the largest scales observable today and super horizon scales, we should expect small anisotropies and inhomogeneities of 1 part in  $10^4 - 10^5$  seeded during inflation. We are however interested in *anomalous anisotropy*, defined as the anisotropy that is much larger than  $10^{-4} - 10^{-5}$  expected from the simplest models of inflation. In this paper we will use word isotropy to mean isotropy in this statistical sense on small scales and absence of anomalously large anisotropy on large scales and not absolute isotropy. The assumption of isotropy and homogeneity in this sense in the cosmological model allows us to treat the small anisotropies and inhomogeneities perturbatively on an

<sup>★</sup> suman2reach@gmail.com

<sup>†</sup> biswap@visva-bharati.ac.in

<sup>‡</sup> khatri@theory.tifr.res.in

absolute isotropic and homogeneous FRW background Universe.

A large number of studies from WMAP and PLANCK (Eriksen et al. 2007; Hoftuft et al. 2009; Akrami et al. 2014; Planck Collaboration et al. 2014a, 2016b; Schwarz et al. 2004; Land & Magueijo 2005; Hanson & Lewis 2009; Moss et al. 2011; Gruppuso et al. 2013; Dai et al. 2013) reveal subtle anomalies in the CMB anisotropies that might challenge the assumption of *statistical isotropy*. Several unexpected features at large angular scales such as a hemispherical power asymmetry and an abnormally large cold spot, although modestly significant, suggest a critical examination of the assumption of isotropy. The assumption of isotropy needs to be tested with independent datasets and with diverse statistical measures. This has been done with various other observations such as the X-ray background (Wu et al. 1999; Scharf et al. 2000), radio sources (Wilson & Penzias 1967; Blake & Wall 2002), Gamma-ray bursts (Meegan et al. 1992; Briggs et al. 1996), supernovae (Gupta & Saini 2010; Lin et al. 2016), galaxies (Marinoni et al. 2012; Gibelyou & Huterer 2012; Yoon et al. 2014; Alonso et al. 2015; Pandey 2017), galaxy clusters (Bengaly et al. 2017) and neutral hydrogen (Hazra & Shafieloo 2015). All these observations are consistent with the assumption of statistical isotropy. Contrary to these findings, there are also other studies with Type-Ia supernovae (Schwarz & Weinhorst 2007; Campanelli et al. 2011; Kalus et al. 2013; Javanmardi et al. 2015; Bengaly et al. 2015), radio sources (Jackson 2012), galaxies (Javanmardi & Kroupa 2017), galaxy luminosity function (Appleby & Shafieloo 2014) and large scale bulk flows (Watkins et al. 2009; Kashlinsky et al. 2008, 2010) which reported statistically significant deviation from isotropy. The current observational status does not provide a clear consensus on the issue of isotropy of the Universe on large scales and further investigations are necessary to either establish or refute it.

The large-scale structures in the Universe emerge from the gravitational collapse of the primordial density fluctuations. The gravitational collapse is anisotropic in nature. In the Zeldovich approximation, an overdense region in the dark matter distribution first collapses along its shortest axis leading to a sheet-like structure (Zeldovich 1970). The subsequent collapse along the medium and the longest axis results in an elongated filament and a dense compact cluster respectively (Shandarin & Zeldovich 1989). Galaxies are a biased tracer of the underlying mass distribution and any anisotropy in the distribution of the dark matter is also expected to be present in the galaxy distribution. The modern redshift surveys like 2dFGRS (Colles et al. 2001) and SDSS (York et al. 2000) have now mapped a large number of galaxies in the local Universe providing an unprecedented view of the galaxy distribution in our neighbourhood. The galaxies are found to be distributed in an interconnected network of filaments, sheets and clusters which are surrounded by large empty regions. The filaments, which acts as interconnecting bridges between the clusters are known to be statistically significant up to  $\sim 70 - 80 h^{-1} \text{Mpc}$  (Bharadwaj et al. 2004; Pandey & Bharadwaj 2005). The Sloan Great Wall discovered in the SDSS (Gott et al. 2005) is one of the richest galaxy system in the nearby Universe and appears to be contiguous over length scales of more than 400 Mpc. Observations suggests that there are voids of enormous sizes such as the Bootes void with radius of 62 Mpc (Kirshner et al.

1987) and the Eridanus supervoid extending up to 300 Mpc (Szapudi et al. 2015). The Eridanus void is also known to be aligned with the CMB cold spot and believed to be associated with it. Observational detection of all these gigantic cosmic structures re-emphasize the necessity of testing the isotropy in the galaxy distribution.

The SDSS is a multiband photometric and spectroscopic redshift survey which covers one quarter of the celestial sphere in the Northern Galactic Cap. The photometric and spectroscopic catalogues of the SDSS now provide redshifts of millions of galaxies making them suitable for testing isotropy in the galaxy distribution. The spectroscopic redshifts are estimated from the spectra of galaxies and hence they are more reliable but difficult and costly to measure for a very large number of galaxies. On the other hand, there is a larger uncertainty in the estimate of the photometric redshifts but photometric data is easier to obtain for a large number of galaxies. Keeping this in mind, we consider both the spectroscopic and photometric catalogues from the SDSS for the present analysis.

Information entropy can be used to test the homogeneity and isotropy of the Universe (Pandey 2013, 2016). In this work, we use an information theory based method (Pandey 2016) to test the isotropy of the local Universe using the spectroscopic and photometric redshift catalogues of the Sloan Digital Sky Survey (SDSS).

A brief outline of the paper follows. We describe the method of analysis in Section 2, the data in Section 3 and present the results and conclusions in Section 4 and Section 5 respectively.

We have used a  $\Lambda$ CDM cosmological model with matter density parameter today, the  $\Omega_{m0} = 0.31$ , dark energy density parameter  $\Omega_{\Lambda 0} = 0.69$  and Hubble parameter  $h = 1$  for converting redshifts to distances throughout the analysis.

## 2 METHOD OF ANALYSIS

We use the anisotropy parameter defined in Pandey (2016) to quantify the anisotropy in the galaxy distribution. This anisotropy parameter uses the information entropy (Shannon 1948) to measure the non-uniformity in the distribution of galaxies. In this method, we first need to divide the entire sky into pixels of equal area and similar shape. The equal area of the pixels ensures that the solid angle subtended by each of these pixels on the observer is the same whereas the similar shapes ensure the same geometry for each of the angular bins. We use the Hierarchical Equal Area isoLatitude Pixelization (HEALPix) software (Górski et al. 1999, 2005) for this purpose. We use the HEALPix resolution parameter  $N_{\text{side}}$  to pixelate the sky into  $N_{\text{pix}} = 12 \times N_{\text{side}}^2$  pixels of equal area. The angular size of each pixel for a specific choice of  $N_{\text{side}}$  is  $\sqrt{\frac{41253}{N_{\text{pix}}}}$  degree where 41253 square degree is the total area of the sky. The angular bins subtended by each of these pixels have the same volumes but may contain different number of galaxies within them. We choose an upper limit  $r_{\text{max}}$  for the radial distance as the galaxies are mapped only within a finite region. Furthermore, the galaxy surveys very often do not provide a full sky coverage. The fact that only a part of the sky is mapped by the survey needs to be taken into account through a mask specific to the survey. The effective number of pixels  $N_{\text{effective}}$  available for the

analysis is smaller than  $N_{\text{pix}}$  and depends on the size and geometry of the mask or the sky coverage of the survey.

We vary the radial distance within the limit  $r_{\text{max}}$  with uniform steps and cumulatively count the number of galaxies within each angular bin. We use a uniform step size of  $10h^{-1}\text{Mpc}$  throughout this analysis. We consider a randomly selected galaxy lying within a radial distance  $r$  from the observer. This galaxy resides in any one of the  $N_{\text{effective}}$  angular bins and the probability of finding the galaxy in any particular bin is proportional to the total number of galaxies residing in that bin. If  $n_i$  is the number of galaxies located in the  $i^{\text{th}}$  angular bin then the probability of finding the galaxy in the  $i^{\text{th}}$  bin is given by,  $f_i = \frac{n_i}{\sum_{i=1}^{N_{\text{effective}}} n_i}$  and  $\sum_{i=1}^{N_{\text{effective}}} f_i = 1$  by definition. So the event of randomly selecting a galaxy has  $N_{\text{effective}}$  outcomes each with a different probability  $f_i$ . The information entropy associated with this event for a specific radial distance  $r$  can be written as,

$$\begin{aligned} H_{lb}(r) &= - \sum_{i=1}^{N_{\text{effective}}} f_i \log f_i \\ &= \log N - \frac{\sum_{i=1}^{N_{\text{effective}}} n_i \log n_i}{N}, \end{aligned} \quad (1)$$

where  $N$  is the total number of galaxies located within a radial distance  $r$  from the observer. The subscript  $lb$  in  $H_{lb}$  implies that we consider the pixels in the longitude-latitude ( $l, b$ ) space and study it as a function of the radial distance  $r$  up to which the number counts are integrated. The base of the logarithm is arbitrary and only decides the unit of information. We use the base of 10 for the present work. If the probabilities  $f_i$  are identical for each of the angular bins then the information entropy will be maximum,  $(H_{lb})_{\text{max}} = \log N_{\text{effective}}$ . This would only occur if each of the angular bins hosts exactly the same number of galaxies within a distance  $r$ . This corresponds to the situation when there is maximum uncertainty about the location of the randomly selected galaxy. We define the anisotropy parameter,

$$a_{lb}(r) = 1 - \frac{H_{lb}(r)}{(H_{lb})_{\text{max}}}, \quad (2)$$

to measure the degree of radial anisotropy present in any distribution. It may be noted that for a completely isotropic distribution, the probability distribution is uniform leading to  $H_{lb}(r) = (H_{lb})_{\text{max}}$  and  $a_{lb}(r) = 0$ . On the other hand, if all the galaxies are located only in one specific bin out of the  $N_{\text{effective}}$  angular bins then the galaxy distribution is maximally anisotropic. In this case, there is no uncertainty about the location of the randomly selected galaxy and consequently we have  $H_{lb}(r) = 0$  and  $a_{lb}(r) = 1$ .

The galaxies are not distributed randomly but in a web-like network. The presence of the coherent patterns in the galaxy distribution like filaments, sheets, clusters and voids cause the distribution to be highly anisotropic on small scales. So the probabilities of locating randomly selected galaxies in different angular bins are not the same. The anisotropy parameter  $a_{lb}(r)$  will measure non-uniformity in the distribution of galaxies as a function of the length scale  $r$ . We will measure the anisotropy parameter  $a_{lb}(r)$  in the SDSS data as a function of  $r$  up to the maximum radial distance  $r_{\text{max}}$ . If the assumption of isotropy on large scales holds in the real Universe then we expect the anisotropy parameter to decrease with the increasing length scale  $r$  and

should become negligibly small on the scales where the Universe becomes isotropic. It should be noted that the value of  $a_{lb}(r)$  is also expected to be sensitive to the choice of  $N_{\text{side}}$  as it decides the total number of pixels  $N_{\text{pix}}$ . The pixel sizes will be larger for a smaller  $N_{\text{side}}$ . As a result the volume covered by each angular bin will be also larger. This would increase the galaxy counts and reduce the Poisson noise leading to a decrease in the anisotropy. Even an isotropic distribution of finite size will exhibit some anisotropy due to the Poisson noise on small scales. To assess this, we compare our results to that obtained from a homogeneous and isotropic Poisson distribution which has the same geometry and sampling density as the actual data.

The anisotropy parameter measured at each length scale for the entire survey region provides the degree of global anisotropy present in the galaxy distribution. Besides the global isotropy, it is also important to compare the degree of anisotropy observed along the different directions in the sky. For this, we will be dividing the SDSS survey area into a small number of regions and separately measure the entropy and anisotropy in each of these regions. This would allow us to test the statistical isotropy of the galaxy distribution and identify the existence of any preferred directions.

The information entropy is related to the higher order moments of a distribution (Pandey 2016), in addition to the second order moment or the power spectrum. The higher order moments of the galaxy density field are expected to be non zero as the present day galaxy distribution is known to be highly non-Gaussian. This provides the argument for using the information entropy as an effective measure of the anisotropy present in the galaxy distribution, since it captures information beyond the 2-point correlation function or the power spectrum.

### 3 DATA

We use the data from the twelfth data release of the Sloan Digital Sky Survey (SDSS, DR12) (Alam et al. 2015) which is the final data release of the SDSS-III. A description of the telescope used in the SDSS is provided in Gunn et al. (2006) and the SDSS camera and filters are discussed in Gunn et al. (1998) and Fukugita et al. (1996) respectively. The target selection algorithm of the Main Galaxy Sample is described in Strauss et al. (2002).

#### 3.1 THE SDSS PHOTOMETRIC DATA

We use the photometric redshift catalogue for the SDSS data prepared by Beck et al. (2016). We select only the galaxies with the photometric error classes 1 and -1 which have accurate redshift error estimates. For other error classes, the redshift estimation errors are dependent on the position in color and magnitude space and hence requires additional statistical errors to be taken into account. We apply a cut in the redshift error estimate  $\delta_z^{\text{photo}} < 0.03$  and consider all the galaxies in the redshift range  $0 < z < 0.3$  with r-band extinction  $A_r < 0.18$  which provides us with a sample containing 2827248 galaxies. Further cuts in the r-band apparent magnitude  $13 < m_r < 19$  and r-band absolute magnitude  $M_r < -20.4$  are applied to construct a volume limited sample

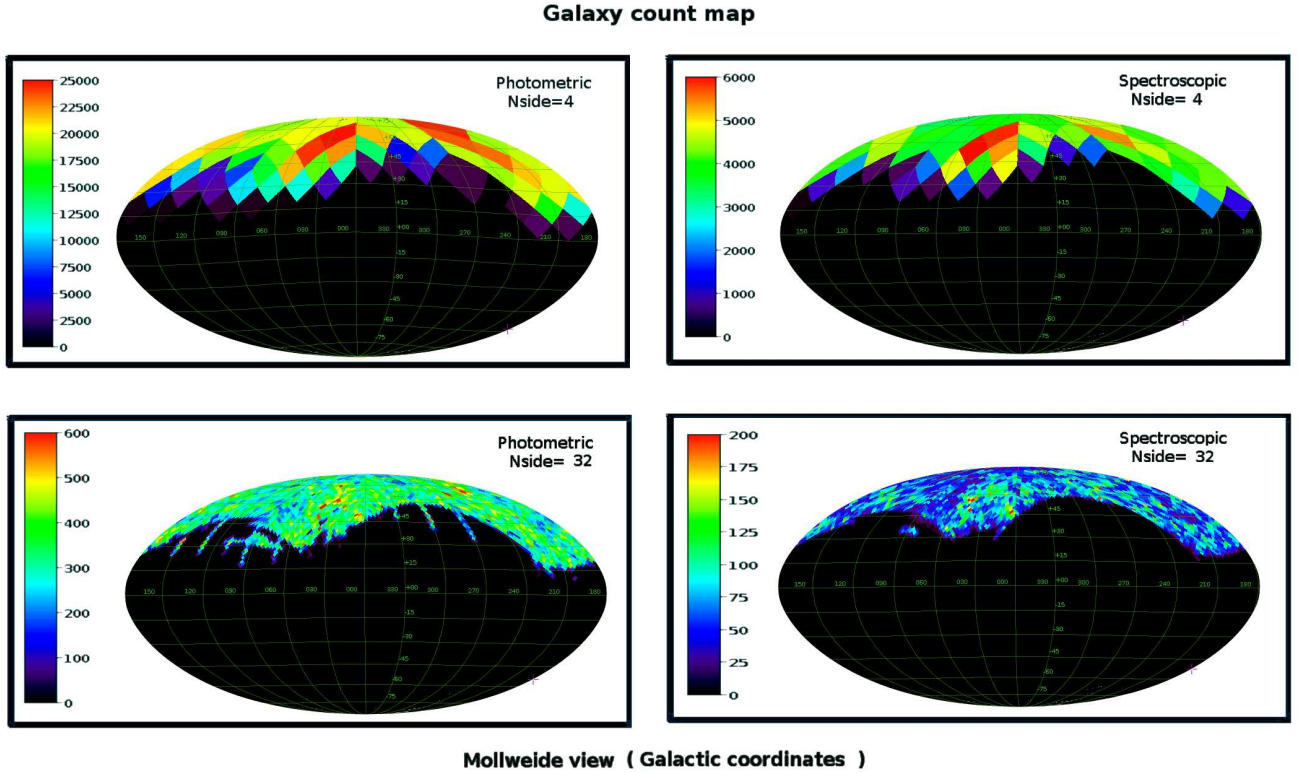


**Figure 1.** The galaxy number counts for the SDSS photometric and spectroscopic samples for two different resolutions, HEALPix  $N_{\text{side}} = 4$  and 32.

of galaxies. The resulting volume limited sample of galaxies extends up to redshift  $z < 0.2143$  or comoving distance  $< 609.197 h^{-1} \text{Mpc}$  and consists of 1022630 galaxies. The volume limited sample prepared from the SDSS photometric data does not start from  $z = 0$  but from  $z = 0.017$  which corresponds to a distance of  $51.4 h^{-1} \text{Mpc}$  due the apparent magnitude cut adopted here. We consider only the galaxies in the Northern Galactic Cap to get a contiguous sky coverage which reduces the available galaxies to 784329 in our volume limited sample.

### 3.2 THE SDSS SPECTROSCOPIC DATA

We use publicly available spectroscopic data from the SDSS CasJobs<sup>1</sup>. We retrieve the spectroscopic information of all the galaxies in the redshift range  $0 < z < 0.3$  yielding 916633 galaxies. We then construct a volume limited sample of galaxies by restricting the r-band Petrosian magnitude in the range  $13 < m_r < 17.77$  and r-band absolute magnitude to  $M_r < -20.4$ . The values of k-corrections are also obtained from the SDSS CasJobs. These cuts yield a volume limited sample of 180181 galaxies distributed within redshift  $z < 0.1341$  or comoving distance  $< 391.8 h^{-1} \text{Mpc}$ . The resulting volume limited sample does not start from  $z = 0$  but from  $z = 0.0167$  due the apparent magnitude range chosen. So the volume limited sample prepared from the SDSS spectroscopic data starts at  $50 h^{-1} \text{Mpc}$  and extends upto

$391.8 h^{-1} \text{Mpc}$ . We require a contiguous region of the sky for our analysis. So we only consider the galaxies in the Northern Galactic Cap which finally leaves us with a volume limited galaxy sample comprised of 152860 galaxies.

### 3.3 PREPARING THE MASKS

We use HEALPix to divide the entire sky into pixels of equal sizes and count the number of galaxies inside each pixel. The galaxy number counts in different pixels for the volume limited samples of galaxies constructed from the spectroscopic and photometric redshift catalogues are shown in Figure 1. The top left and bottom left panels of Figure 1 show the number counts in the SDSS photometric data with  $N_{\text{side}} = 4$  and  $N_{\text{side}} = 32$  respectively. The top right and bottom right panels show the same but for the SDSS spectroscopic data. The galaxy distributions are 3-dimensional and these counts are the integrated galaxy counts inside each pixel up to the maximum radial extent of the corresponding galaxy samples.  $N_{\text{side}}$  sets the resolution of the map. As a result we see relatively smaller number counts inside the pixels for  $N_{\text{side}} = 32$  than  $N_{\text{side}} = 4$ . It may be also noted that the pixels near the boundary of the survey regions preferentially show lower number counts. This is related to the fact that only parts of the boundary pixels lie inside the survey region. These pixels need to be discarded from any analysis of isotropy and we take this into account by preparing a mask for each dataset and for each resolution.

To prepare the mask we sub-pixelate each pixel into smaller sub-pixels using a new variable  $N_{\text{side}}^{\text{sub}}$  which we have

<sup>1</sup> <http://skyserver.sdss.org/casjobs/>

taken to be  $N_{\text{side}}^{\text{sub}} = 64$  for the present work. We count galaxies inside each of the sub-pixels and create a mask map by assigning a value 1 to the non-empty sub-pixels and 0 to the empty sub-pixels. We then degrade the mask map to a new mask map for  $N_{\text{side}}$ . The pixels for which all the sub-pixels are empty have value 0 and are masked. The values for pixels at the boundary indicate the fraction of non-empty sub-pixels in that pixel. We identify and mask the sparsely populated pixels near the boundary by using a threshold value  $m_{\text{th}}$  for this map. If a pixel in the  $N_{\text{side}}$  map has a value  $< m_{\text{th}}$  then we mask the corresponding pixel. In our analysis we have used  $m_{\text{th}} = 0.75$ .

### 3.4 RANDOM MOCK CATALOGUES

We generate 10 Poisson random distributions for both the volume limited samples constructed from the spectroscopic and photometric data. The mean density of these samples is chosen to be same as the respective volume limited samples under consideration. We then apply the respective masks to generate 10 random mock catalogues each for the SDSS spectroscopic and photometric samples.

### 3.5 MOCK CATALOGUES FROM N-BODY SIMULATIONS

We use a Particle-Mesh (PM) N-Body code to simulate the present day distributions of dark matter in the  $\Lambda$ CDM model. We use  $\Omega_{m0} = 0.31$ ,  $\Omega_{\Lambda0} = 0.69$ ,  $h = 0.68$ ,  $\sigma_8 = 0.81$  and  $n_s = 0.96$  (Planck Collaboration et al. 2016a) as the values of the cosmological parameters. We simulate the distributions using  $256^3$  particles on a  $512^3$  grid in a comoving volume of  $(1433.6h^{-1}\text{Mpc})^3$ . We run the simulations for three different realizations of the initial density fluctuations. We place an observer inside the centre of each simulation box and map the distributions to redshift space using the peculiar velocities of particles. The individual particles are treated as galaxies and we construct 3 mock catalogues from each of the three boxes for each of the two volume limited SDSS samples (photometric and spectroscopic) by sampling particles with the same mean density as the corresponding SDSS sample and applying the respective masks. This provides us with 9 mock galaxy catalogues for the  $\Lambda$ CDM model for each of the volume limited SDSS samples.

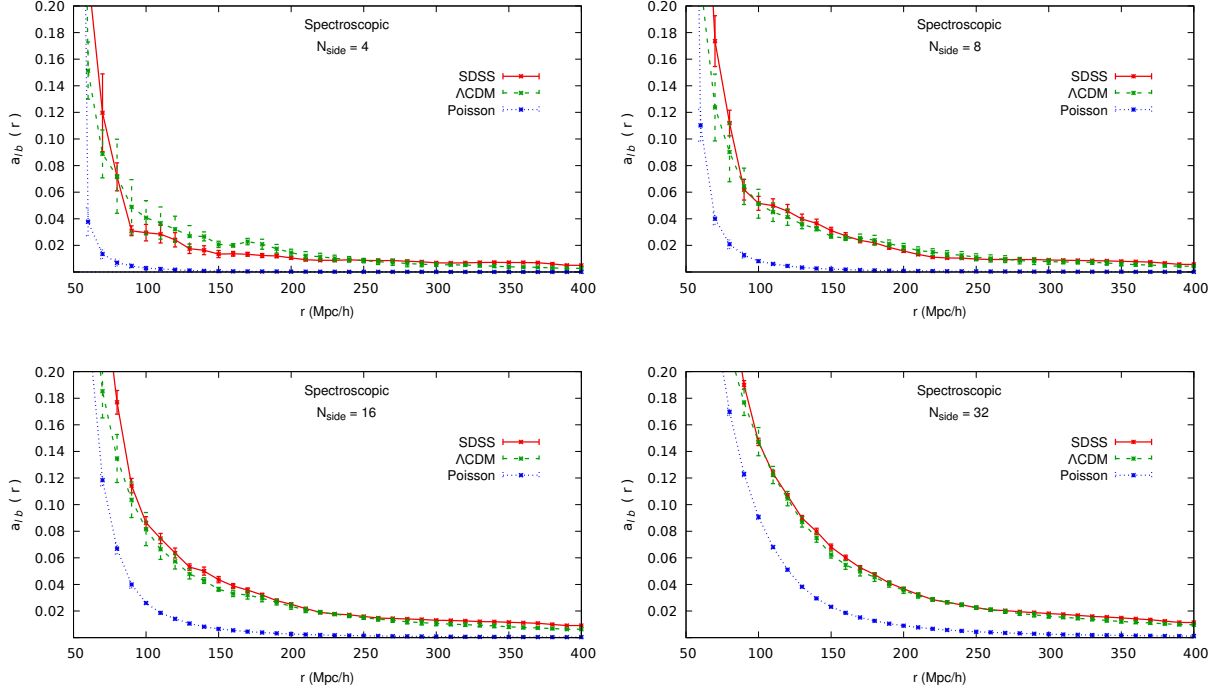
## 4 RESULTS

### 4.1 THE GLOBAL ANISOTROPY IN THE PHOTOMETRIC AND SPECTROSCOPIC GALAXY SAMPLES

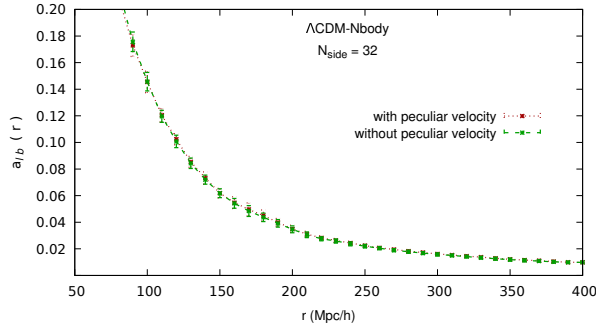
We measure the anisotropy parameter  $a_{lb}(r)$  defined in Equation 1 using all the pixels inside the unmasked region of the sky. We separately measure the anisotropy in the photometric and the spectroscopic datasets from the SDSS at four different resolutions with HEALPix  $N_{\text{side}} = 4, 8, 16$  and 32. The corresponding mock galaxy catalogues from the random distributions and the N-body simulations of the  $\Lambda$ CDM model are also analyzed at the same resolution for comparison. The results for the spectroscopic and photometric data are shown in Figure 2 and Figure 4 respectively. The top left panel of

Figure 2 shows the variation of the anisotropy parameter  $a_{lb}(r)$  as a function of distance for the SDSS spectroscopic data for  $N_{\text{side}} = 4$ . The results for the mock galaxy catalogues from the random distributions and the N-body simulations of the  $\Lambda$ CDM model are also shown together in this panel for comparison with the observations. The  $1-\sigma$  errorbars for the SDSS data are estimated from the 10 Jackknife samples drawn from the data. The  $1-\sigma$  errorbars for the mock catalogues from the random distributions and the  $\Lambda$ CDM model are estimated from 10 and 9 independent realizations respectively. The top right, bottom left and bottom right panels of Figure 2 show the same quantities but for  $N_{\text{side}} = 8, 16$  and 32 respectively. In each of these panels we see that the galaxy distribution in the SDSS is highly anisotropic on small scales. The observed anisotropy in the galaxy distribution decreases with increasing length scales. It is interesting to note that the mock galaxy catalogues from the  $\Lambda$ CDM N-body simulations reproduce the observed anisotropy in the SDSS data remarkably well for each value of  $N_{\text{side}}$ . The anisotropy observed in the mock catalogues from the random distributions also decreases with increasing length scales but the degree of anisotropy observed in these cases are noticeably smaller than the SDSS and  $\Lambda$ CDM. The anisotropy observed in the random distributions are sourced by only the Poisson noise which naturally decreases with increasing length scales due to the increase in galaxy counts at larger scales. On the other hand the anisotropies in the galaxy distribution in the SDSS and the  $\Lambda$ CDM model are sourced by both the Poisson noise and anisotropic gravitational clustering. The effect of Poisson noise on the anisotropy is expected to diminish with increasing galaxy counts in similar manner in all 3 datasets but the additional anisotropy present in the SDSS and  $\Lambda$ CDM model due to the gravitational clustering would change differently depending on the nature and strength of clustering present in them. We find that the anisotropies in the SDSS and the  $\Lambda$ CDM model decreases to a small value and plateaus out beyond a length scale of  $200h^{-1}\text{Mpc}$ . Since the  $\Lambda$ CDM simulations assume an isotropic background and statistically isotropic initial perturbations, the comparison of the data with simulations tests the validity of these assumptions. The difference between the simulations and data in particular becomes negligible at scales  $r \gtrsim 200\text{Mpc}/h$ .

There is excess residual anisotropy, over the isotropic Poisson samples, present in the SDSS data and the  $\Lambda$ CDM simulations. The two contributions to the anisotropy in the observed data come from clustering in real space and from the effect of peculiar velocities on the redshift measurements, the so called redshift space distortions. The SDSS galaxies are mapped in redshift space where the peculiar velocities perturb the redshifts and distort the galaxy distribution. The large scale coherent inflow towards the overdense regions and outflow from the underdense regions introduce specific anisotropic features in clustering pattern of the galaxies. Also, the random peculiar velocities inside the virialized bound structures elongate the structures along the line of sight giving rise to what is popularly known as the ‘‘Fingers of God (FOG)’’ effect. Since we integrate along the radial direction, the errors in distance measurements coming from peculiar velocities should get averaged out. We therefore do not expect the redshift space distortions to contribute significantly to our anisotropy parameter  $a_{lb}$ . For



**Figure 2.** The anisotropy parameter  $a_{lb}(r)$  measured as a function of radial distance  $r$  for SDSS spectroscopic data along with the same for the mock galaxy catalogues drawn from the random distributions and N-body simulations of the  $\Lambda$ CDM model. Each panel shows the results for a different resolution of the maps decided by the value of  $N_{\text{side}}$  indicated in that panel.  $1-\sigma$  errorbars shown on each SDSS data points are estimated from the 10 Jackknife samples drawn from the data. The  $1-\sigma$  errorbars for the  $\Lambda$ CDM model and Poisson random distribution are estimated from 9 and 10 independent realizations respectively.



**Figure 3.** Comparison of the anisotropy parameter  $a_{lb}(r)$  of the mock galaxy samples when they are prepared with and without taking into account the effect of peculiar velocities (redshift space distortions). The  $1-\sigma$  errorbars shown are estimated using 10 independent realizations.

the same reason, our results are also insensitive to the errors in redshifts, especially in the photometric sample. We can explicitly check this using the mock catalogues from the N-body simulations. We separately construct 10 mock galaxy catalogues for the SDSS spectroscopic sample from the  $\Lambda$ CDM N-body simulations without taking into account the effect of peculiar velocities, i.e. without the redshift space distortions. We measure the anisotropy parameter  $a_{lb}(r)$  in these samples and compare the results with that for the mock galaxy samples prepared by taking into account the effect of peculiar velocities, as in real observations. The results are shown in Figure 3. We find that the anisotropy

parameter  $a_{lb}(r)$  is insensitive to the redshift space distortions. So the small residual anisotropy on large scales are not sourced by the random peculiar velocities inside FOGs. The remaining small difference in anisotropy between the galaxy distribution and the Poisson distribution indicates that the galaxy distribution can not be represented by a Poisson distribution on any length scale. We should expect this just from linear growth. The scales of 200 Mpc entered horizon around  $z \approx 1000$  with an amplitude of  $\sim 10^{-5}$  and would have grown by a factor of  $\sim 1000$  today to an amplitude of  $\sim 10^{-2}$ . This is also the level of anisotropy that we see in  $a_{lb}$ . We will show explicitly below that this resid-

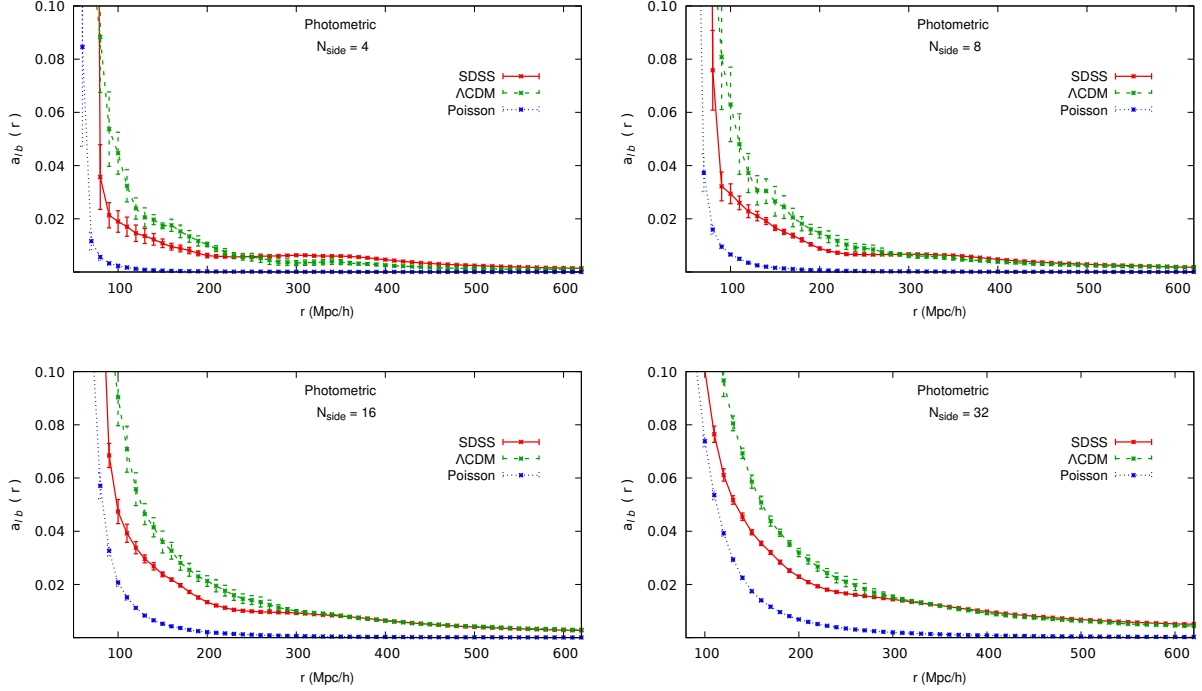


Figure 4. Same as Figure 2 but for the SDSS photometric data.

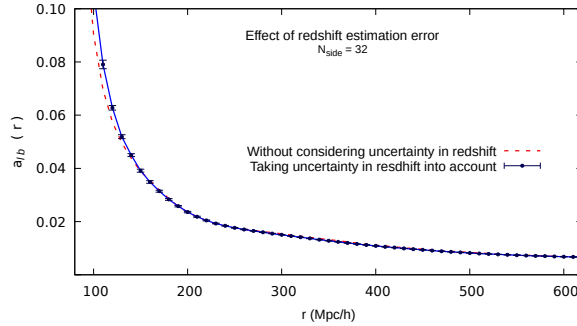
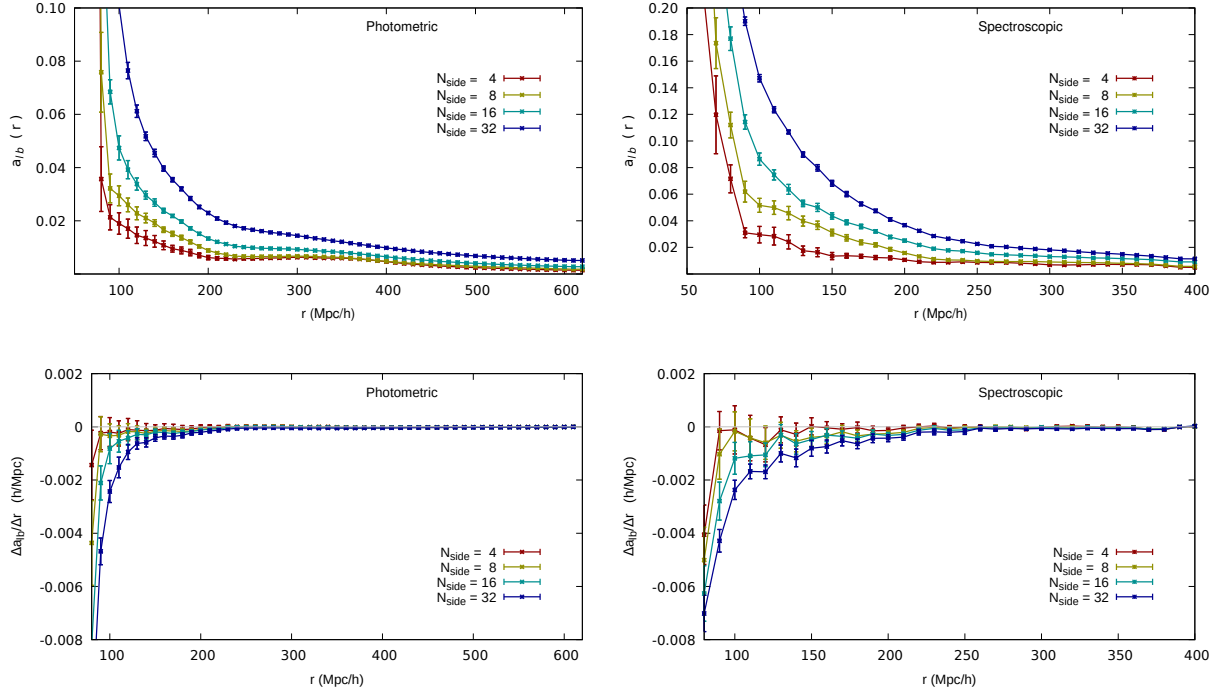


Figure 5. Effect of the uncertainty in the measurements of the photometric redshifts (Beck et al. 2016) in the SDSS. The  $1-\sigma$  errorbars shown are estimated using 10 independent realizations. The anisotropy parameter  $a_{lb}$  is insensitive to small errors in the photometric redshift estimates.

ual anisotropy is nothing but the linear large scale structure in the  $\Lambda$ CDM universe and comparison with linear theory defines an unambiguous scale of isotropy.

We also analyze the SDSS photometric data exactly in the same way and present our results in Figure 4. The SDSS photometric sample covers a much larger volume and hence contains a significantly larger number of galaxies. Interestingly, we find that the results are very similar to those found with the SDSS spectroscopic sample. The anisotropy in the galaxy distribution decreases with length scale in each case and the galaxy distribution appears to be nearly isotropic beyond a length scale of  $200h^{-1}$  Mpc. We note that the anisotropies observed in the SDSS photometric sample are relatively smaller than what is predicted by the dark matter only  $\Lambda$ CDM simulations on scales below  $200h^{-1}$  Mpc i.e the distribution of the galaxies in the local Universe is

more uniform than the expectations from the  $\Lambda$ CDM model. But interestingly the anisotropy curves for both the distributions flatten out on the same scales. The differences between the observed anisotropy in the SDSS photometric data and the  $\Lambda$ CDM model may arise due to the larger uncertainties associated with the photometric redshifts in the SDSS. We test this possibility using the redshift estimation errors provided by Beck et al. (2016). Beck et al. (2016) use a linear fit in colour magnitude space to describe the photometric redshift and estimate the rms error  $\delta z_{phot,i}$  in photometric redshift measurement for each galaxies. We draw the errors on the photometric redshift for each galaxy from Gaussians with standard deviations  $\delta z_{phot,i}$  and simulate a set of galaxy catalogues from the primary SDSS photometric redshift catalogue. We construct 10 volume limited galaxy samples from these datasets and analyze them separately.



**Figure 6.** The anisotropy parameter  $a_{lb}(r)$  for the SDSS photometric and spectroscopic data as a function of radial distance for different  $N_{side}$  values used for analysis. The bottom panels show the rate of change of the anisotropy in each case as measured by the slopes of the curves shown in the top panels.

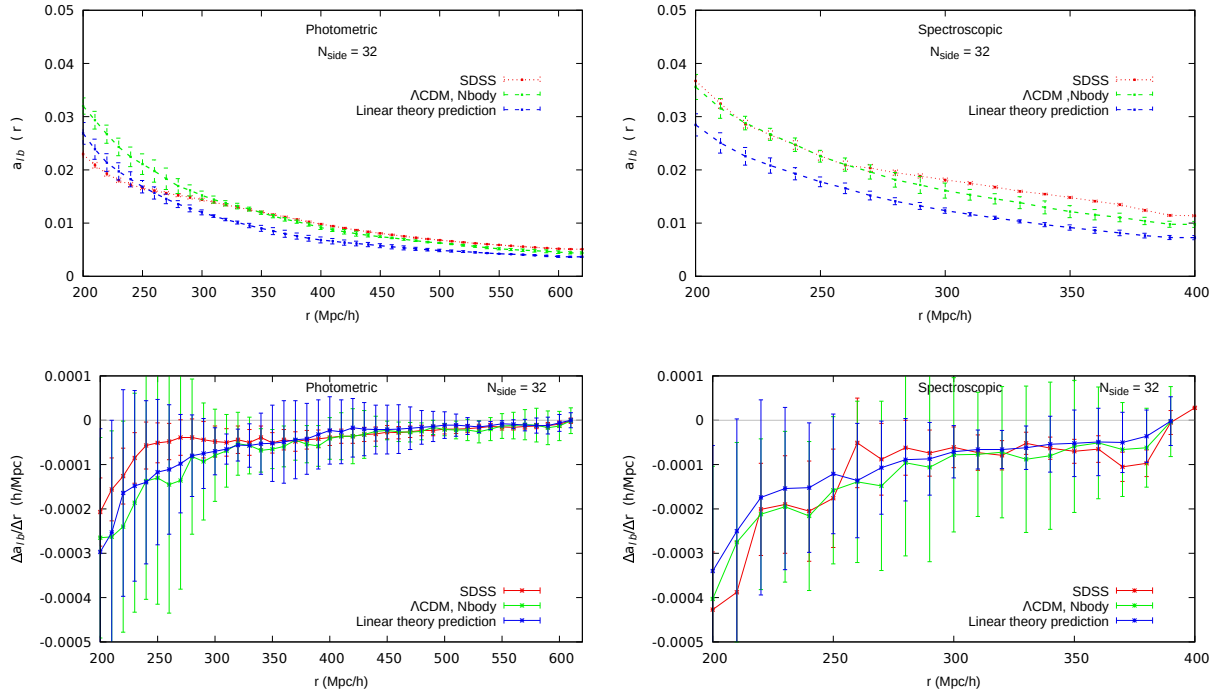


**Figure 7.** The top left panel compares the residual anisotropy on large scales observed in the SDSS photometric sample,  $\Lambda$ CDM N-body simulations and that expected from the linear theory. The top right panel compares the same for the SDSS spectroscopic sample. The bottom left panel shows the variation of slopes of the anisotropy parameter as a function of length scales for the SDSS photometric sample along with the predictions from the  $\Lambda$ CDM N-body simulations and linear theory. The right panel compares the same but for the SDSS spectroscopic sample. The  $1-\sigma$  errorbars shown in each case are estimated using 10 independent realizations.

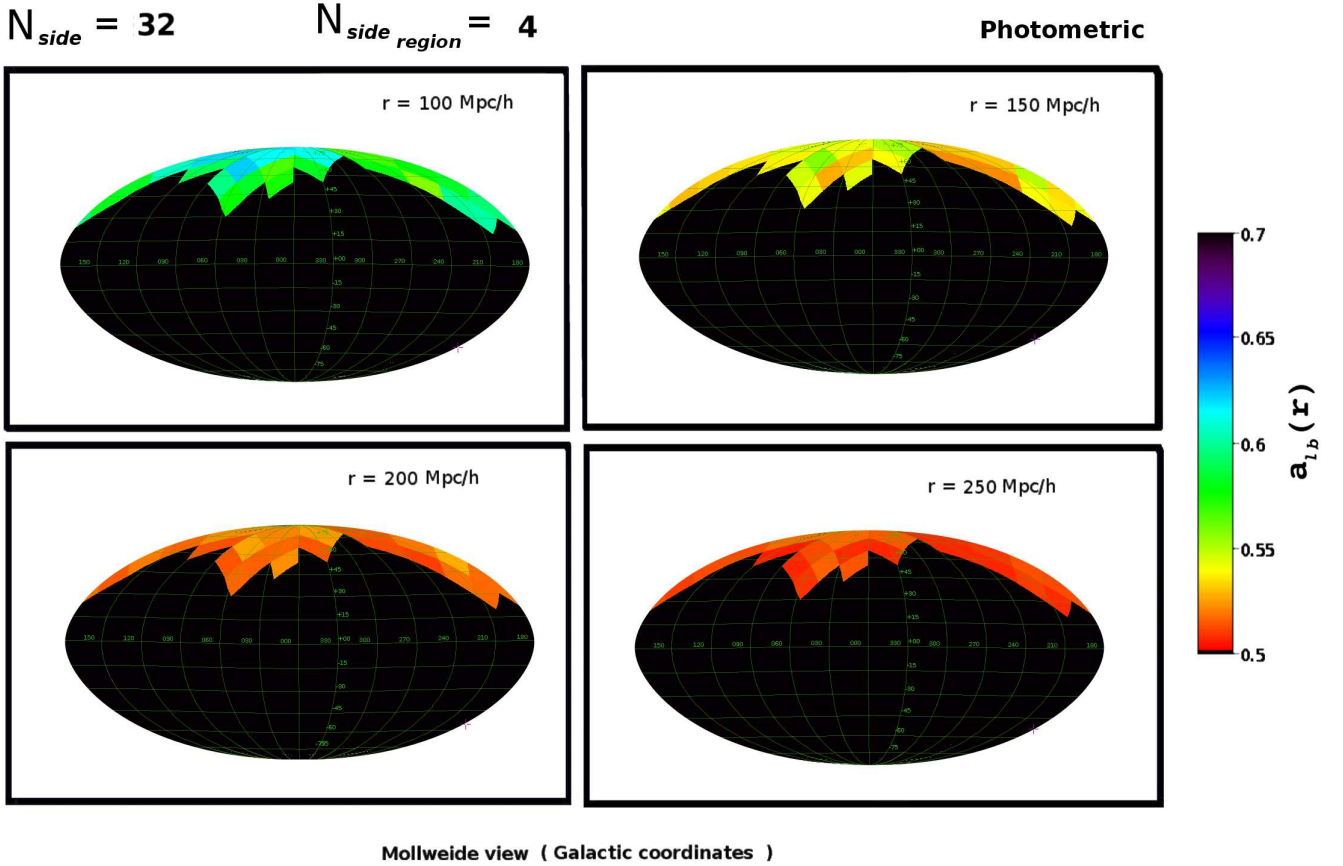


**Figure 8.** The anisotropy parameter  $a_{lb}(r)$  in the 23 separate regions of the SDSS photometric sky at different radii  $r$ . The pixelization is done with  $N_{side} = 32$  for calculating  $a_{lb}$  in each region, with each region corresponding to a pixel of  $N_{side}^{region} = 4$  HEALPix map.

The results are presented in Figure 5 which indicates that the uncertainty in the measurement of photometric redshift is unlikely to change the anisotropy. As stated above, this is expected since we integrate along the line of sight and any errors in redshift estimates would average out, similar to the effect of the peculiar velocities. The difference in dark matter only simulations and SDSS data is therefore mostly because of the baryonic astrophysics. However, further investigations are necessary to either support or refute this claim. One may also note an apparent increase in the anisotropy at  $\sim 300h^{-1}\text{Mpc}$  for  $N_{side} = 4$  and  $N_{side} = 8$  which may arise due to the presence of a large supercluster or void at this distance.

In the top left and right panels of Figure 6, we compare the anisotropy in the SDSS photometric and spectroscopic galaxy samples respectively for different  $N_{side}$ . We observe a larger degree of anisotropy in the galaxy distribution at higher resolution due to a larger contribution from the Poisson noise. We show the rate of change of anisotropy in each case for the photometric and spectroscopic data in the bottom left and right panels of Figure 6 respectively. We find that for both the SDSS photometric and spectroscopic data, the observed slopes flattens out nearly to zero on scales of  $\sim 100h^{-1}\text{Mpc}$  for  $N_{side} = 4$  and 8. The same trend is observed on  $\sim 200h^{-1}\text{Mpc}$  for  $N_{side} = 16$  and 32 for both the datasets.

We linearly evolve the initial power spectrum upto

present day and then use it to generate particle distributions at present within the N-body cube. These distributions represent the linear version of the present day mass distribution. We generate 3 such distributions and construct 10 independent mock samples for the spectroscopic and photometric sample from these distributions. We analyzed them in exactly same manner and find that a nearly constant residual anisotropy of the order of  $10^{-2}$  persists on large scales irrespective of the chosen value of  $N_{side}$ . The top two panels of Figure 7 show that there is a small offset between the residual anisotropy observed in the SDSS and that predicted by linear theory. The residual anisotropy in the  $\Lambda\text{CDM}$  mock catalogues are consistent with the SDSS observations.

We will use the slope of the anisotropy parameter  $a_{lb}$ , which is a local quantity and insensitive to the overall normalization and therefore cosmological parameters, to define the scale of isotropy.

In Figure 6, we see that for any  $N_{side}$ , the anisotropy parameter eventually plateaus out to a small value ( $\sim 10^{-2}$ ) on a certain scale and the corresponding slope of the anisotropy parameter tends to zero. However it may be noted that the slope of the anisotropy parameter does not become exactly zero on any length scales. In the two bottom panels of Figure 7, we blow up the y-axes representing the slopes of the anisotropy parameter and find that the slopes are of the order of  $10^{-4} h/\text{Mpc}$  beyond a length scale of  $200h^{-1}\text{Mpc}$  for

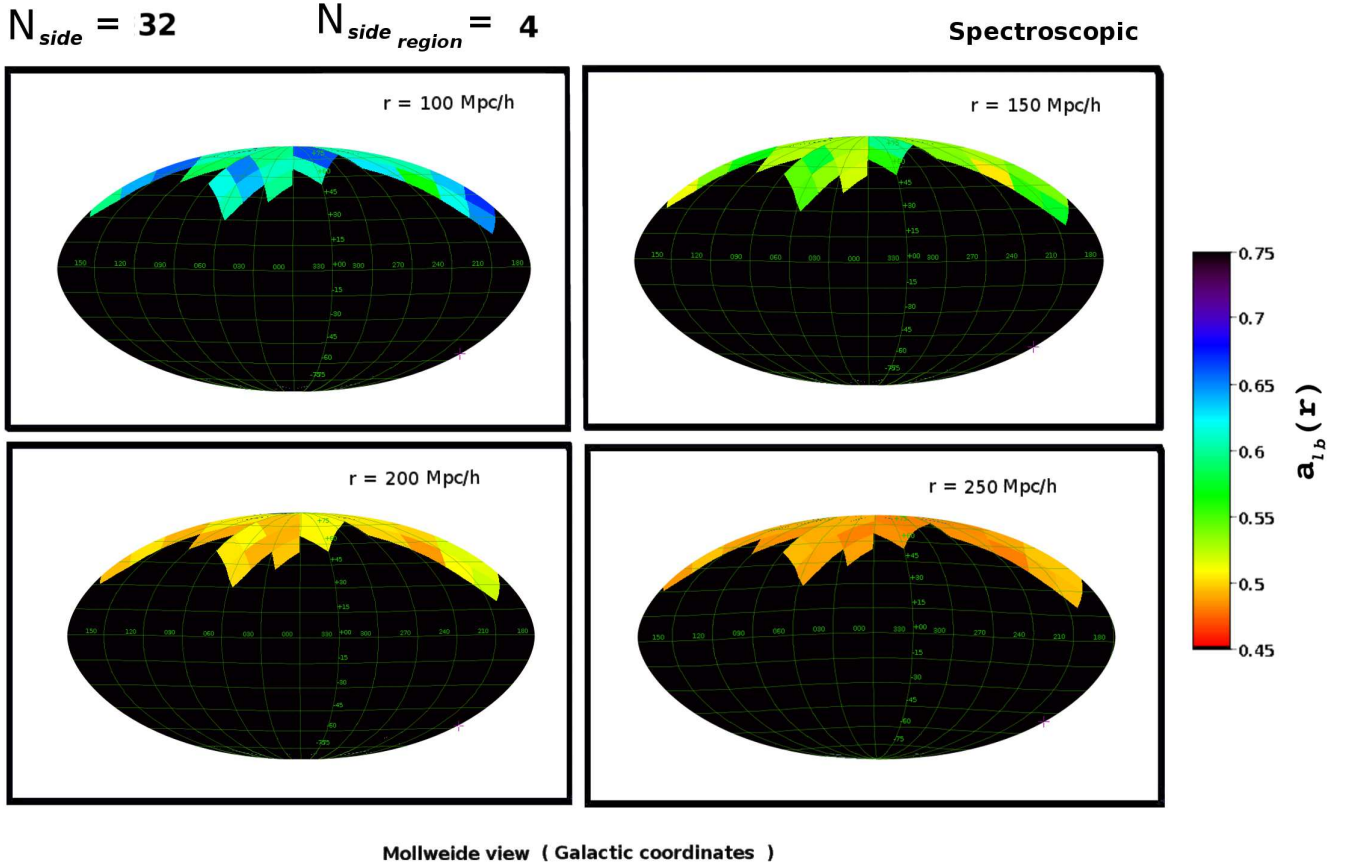


**Figure 9.** Same as Figure 8 but for the SDSS spectroscopic sky. The effective number of independent regions in this case is 22.

both the photometric and spectroscopic sample. We calculate the slopes of the anisotropy curves expected in linear theory and compare them to the observed values in Figure 7 for  $N_{\text{side}} = 32$ . We find that the slopes of the anisotropy curves for both the photometric and spectroscopic samples come within  $1 - \sigma$  errorbars of the slopes expected from the linear theory beyond a length scale of  $\sim 200 h^{-1}$  Mpc. We thus conclude that the anisotropy decays in the same way as predicted by the linear theory beyond  $r \sim 200 h^{-1}$  Mpc. We note that the anisotropy parameter  $a_{lb}$  has contributions from all scales while the slope is a local quantity and is only sensitive to the scale at which it is being calculated. We therefore use the slope as the criteria to define the scale of isotropy yielding a scale of isotropy of  $\sim 200 h^{-1}$  Mpc.

#### 4.2 THE STATISTICAL ISOTROPY IN THE PHOTOMETRIC AND SPECTROSCOPIC GALAXY SAMPLES

Besides measuring the global isotropy across the entire contiguous region of the SDSS photometric and spectroscopic data, we also quantify local anisotropy in smaller regions of the sky and study how it varies over the survey area. We divide the survey area into smaller regions with each *region* defined as a pixel of HEALPix resolution  $N_{\text{side}}^{\text{region}} = 4$  and use resolution of  $N_{\text{side}} = 32$  to study isotropy in each region individually. We obtain 23 and 22 regions in the SDSS pho-

tometric and spectroscopic survey areas respectively. The galactic co-ordinates of these pixels are tabulated in Table A1 in the Appendix. We then compute the degree of anisotropy in each region by calculating the entropy associated with the counts in all  $N_{\text{side}} = 32$  pixels inside each region. We show the maps of  $a_{lb}$  for the SDSS photometric and spectroscopic data at different radial distances in Figure 8 and Figure 9 respectively. The radial distance provided in each panel of these figures indicates the maximum radial distance up to which the galaxy counts are integrated to calculate the anisotropy inside each region. It may be noted that at a given length scale, these anisotropies are relatively higher as compared to the global anisotropies observed in the bottom right panels of Figure 2 and Figure 4. This is simply due to the smaller sample size in each region compared to the full survey area and therefore larger Poisson noise. We find that both the photometric and spectroscopic SDSS sky show significant variations in the measured anisotropy across different regions of the sky at a radial distance of  $100 h^{-1}$  Mpc. The variations in the local anisotropy across regions decrease with increasing length scales and nearly cease to exist at  $\sim 200 h^{-1}$  Mpc.

In Figure 10, we also show the variation in the anisotropy parameter  $a_{lb}(r)$  with distance  $r$  for each of the individual 23 and 22 regions in the photometric and spectroscopic data respectively. The observed anisotropy in each region is higher compared to the full survey due to the larger

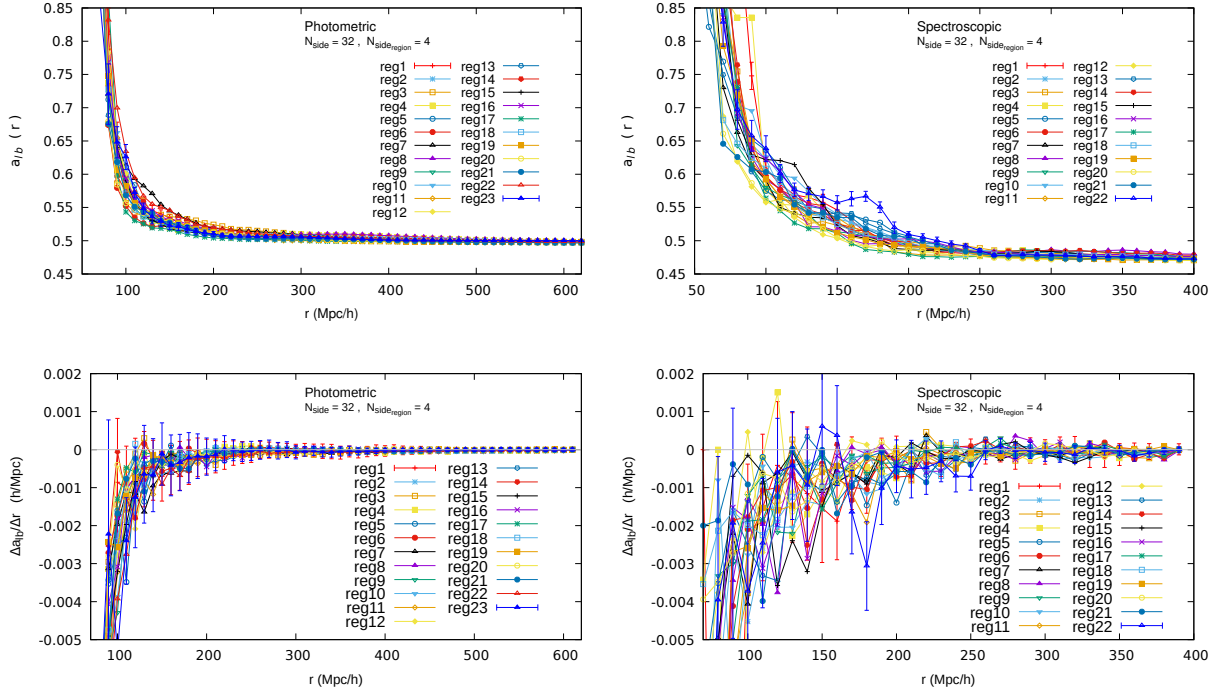


**Figure 10.** The top left and right panels show anisotropy  $a_{lb}(r)$  as a function of radial distance  $r$  for each independent region, with each region corresponding to a HEALPix pixel in  $N_{\text{side}} = 4$  map, in the SDSS photometric and spectroscopic sky respectively. The two bottom panels show the rate of change of anisotropy with  $r$  in each pixels/regions of the respective datasets. The  $1-\sigma$  errorbars in each case are estimated from the 10 Jackknife samples drawn from the data.

Poisson noise in each smaller regions. The bottom panels shows the rate of change of anisotropy in each of these 23/22 regions. The results shown in Figure 10 indicate that different parts of the SDSS photometric and spectroscopic sky exhibit similar degree of anisotropy beyond a length scale of  $\sim 200h^{-1}\text{Mpc}$  after which the anisotropy parameter  $a_{lb}$  is approximately constant. We do not find any significantly divergent pixel beyond a length scale of  $200h^{-1}\text{Mpc}$ . This suggests that the galaxy distribution mapped by the SDSS in both the photometric and spectroscopic redshift survey is isotropic on a length scale of  $200h^{-1}\text{Mpc}$  and there are no preferred directions in the SDSS survey volume beyond this length scale.

## 5 CONCLUSIONS

In this work, we have analyzed the SDSS photometric and spectroscopic data with information entropy to test the isotropy of the galaxy distribution in the local Universe. We find that the galaxy distribution is highly anisotropic on small scales but these anisotropies decrease with increasing radial distances. The anisotropies predicted by the  $\Lambda\text{CDM}$  N-Body simulations are in fairly good agreement with the observed anisotropies with the SDSS. Both photometric and spectroscopic data from SDSS exhibit a small residual anisotropy on large scales. The  $\Lambda\text{CDM}$  simulations accurately reproduce the small residual anisotropy observed on large scales. These residual anisotropies on large scales are expected just from the linearly evolved primordial anisotropies. To verify this, we also study the anisotropies in

the distributions generated from a linearly evolved  $\Lambda\text{CDM}$  power spectrum and find a residual anisotropy of the same order as observed in the SDSS and  $\Lambda\text{CDM}$  N-body simulations. We find a small offset in the magnitude of the residual anisotropy observed in the  $\Lambda\text{CDM}$  N-Body simulations and the linear theory. We show that this offset originates from the differences in the mass variance in the two distributions on the corresponding length scales. To avoid the complications associated with the offsets and normalization of the fluctuations which would be a function of cosmological parameters, we use the slope of the anisotropy, a local quantity, to define the scale of isotropy. We study the slopes of the anisotropy parameter as a function of length scales in the SDSS and linear theory and find that the slopes agree with each other at  $1-\sigma$  level beyond a length scale of  $200h^{-1}\text{Mpc}$  indicating the onset of isotropy. To be precise, the decay in anisotropy parameter  $a_{lb}$  is consistent beyond this scale with the linear perturbation theory expectation.

It may be noted that the degree of residual anisotropy depends on the value of  $N_{\text{side}}$  (Figure 6) which decides the size of the angular patches or the volumes subtended by them at the observer. The value of  $N_{\text{side}}$  controls the magnitude of the shot noise and hence the anisotropy. We find that irrespective of the choice of  $N_{\text{side}}$ , the galaxy distribution shows a transition to isotropy on large scales. We would like to clarify here that the *length scale* throughout our analysis refers to the farthest distance along the radial direction up to which the number counts are integrated.

An analysis of the Luminous Red Galaxies (LRG) from the SDSS DR7 by Marinoni et al. (2012) find the scale of isotropy to be  $150h^{-1}\text{Mpc}$  which is somewhat different than

the value obtained in this work. The LRG sample analyzed by [Marinoni et al. \(2012\)](#) span a redshift range  $0.22 < z < 0.5$  whereas the SDSS galaxy samples analyzed here are limited to redshift  $z < 0.21$ . So the difference in the result arises both due to different magnitude limits of the samples and different methods of analysis.

We test for the statistical isotropy by separately measuring anisotropy in different sub-samples/regions of the SDSS survey and find no evidence for a preferred direction beyond the scale  $200h^{-1}$  Mpc.

Our analysis indicates that the galaxy distribution shows a transition to isotropy on a scale  $\sim 200h^{-1}$  Mpc for both the SDSS photometric and spectroscopic data. We conclude from the present analysis that the galaxy distribution in the local Universe is indeed isotropic on a scale of  $200h^{-1}$  Mpc which reaffirms the validity of the assumption of isotropy of the Universe on large scales.

## 6 ACKNOWLEDGEMENT

The authors thank an anonymous reviewer for useful comments and suggestions. The authors would like to thank the SDSS team for making the data public. The authors would like to thank Maciej Bilicki for providing the SDSS photometric catalogue. BP would also like to thank Maciej Bilicki for helpful comments and suggestions on the draft. SS would like to thank UGC, Government of India for providing financial support through a Rajiv Gandhi National Fellowship. B.P. would like to acknowledge financial support from the SERB, DST, Government of India through the project EMR/2015/001037. B.P. would also like to acknowledge IUCAA, Pune and CTS, IIT, Kharagpur for providing support through associateship and visitors programme respectively. RK was supported by SERB grant number ECR/2015/000078 from Science and Engineering Research Board, Department of Science and Technology, Govt. of India and by MPG-DST partner group between Max Planck Institute for Astrophysics and Tata Institute of Fundamental Research, Mumbai funded by Max Planck Gesellschaft, Germany.

## REFERENCES

- Akrami, Y., Fantaye, Y., Shafieloo, A., et al. 2014, *ApJ Letters*, 784, L42
- Alam, S., Albareti, F. D., Allende Prieto, C., et al. 2015, *ApJS*, 219, 12
- Alonso, D., Salvador, A. I., Sánchez, F. J., et al. 2015, *MNRAS*, 449, 670
- Appleby, S., & Shafieloo, A. 2014, *JCAP*, 10, 070
- Beck, R., Dobos, L., Budavári, T., Szalay, A. S., & Csabai, I. 2016, *MNRAS*, 460, 1371
- Bengaly, C. A. P., Jr., Bernui, A., & Alcaniz, J. S. 2015, *ApJ*, 808, 39
- Bengaly, C. A. P., Bernui, A., Ferreira, I. S., & Alcaniz, J. S. 2017, *MNRAS*, 466, 2799
- Bharadwaj, S., Bhavsar, S. P., & Sheth, J. V. 2004, *ApJ*, 606, 25
- Blake, C., & Wall, J. 2002, *Nature*, 416, 150
- Briggs, M. S., Paciesas, W. S., Pendleton, G. N., et al. 1996, *ApJ*, 459, 40
- Campanelli, L., Cea, P., Fogli, G. L., & Marrone, A. 2011, *Physical Review D*, 83, 103503
- Carlstrom, J. E., Ade, P. A. R., Aird, K. A., et al. 2011, *PASP*, 123, 568
- Crill, B. P., Ade, P. A. R., Artusa, D. R., et al. 2003, *ApJS*, 148, 527
- Colles, M. et al. (for 2dFGRS team) 2001, *MNRAS*, 328, 1039
- Dai, L., Jeong, D., Kamionkowski, M., & Chluba, J. 2013, *Physical Review D*, 87, 123005
- Eriksen, H. K., Banday, A. J., Górski, K. M., Hansen, F. K., & Lilje, P. B. 2007, *ApJ Letters*, 660, L81
- Fixsen, D. J., Cheng, E. S., Gales, J. M., et al. 1996, *ApJ*, 473, 576
- Fowler, J. W., Niemack, M. D., Dicker, S. R., et al. 2007, *Appl. Opt.*, 46, 3444
- Fukugita, M., Ichikawa, T., Gunn, J. E., et al. 1996, *AJ*, 111, 1748
- Gibelyou, C., & Huterer, D. 2012, *MNRAS*, 427, 1994
- Górski, K. M., Wandelt, B. D., Hansen, F. K., Hivon, E., & Banday, A. J. 1999, *arXiv:astro-ph/9905275*
- Górski, K. M., Hivon, E., Banday, A. J., et al. 2005, *ApJ*, 622, 759
- Gott, J. R., III, Jurić, M., Schlegel, D., et al. 2005, *ApJ*, 624, 463
- Gruppuso, A., Natoli, P., Paci, F., et al. 2013, *JCAP*, 7, 047
- Gupta, S., & Saini, T. D. 2010, *MNRAS*, 407, 651
- Gunn, J. E., Carr, M., Rockosi, C., et al. 1998, *AJ*, 116, 3040
- Gunn, J. E., Siegmund, W. A., Mannery, E. J., et al. 2006, *AJ*, 131, 2332
- Hanson, D., & Lewis, A. 2009, *Physical Review D*, 80, 063004
- Hazra, D. K., & Shafieloo, A. 2015, *JCAP*, 11, 012
- Hoftuft, J., Eriksen, H. K., Banday, A. J., et al. 2009, *ApJ*, 699, 985
- Jackson, J. C. 2012, *MNRAS*, 426, 779
- Javanmardi, B., Porciani, C., Kroupa, P., & Pflamm-Altenburg, J. 2015, *ApJ*, 810, 47
- Javanmardi, B., & Kroupa, P. 2017, *A&A*, 597, A120
- Kalus, B., Schwarz, D. J., Seikel, M., & Wiegand, A. 2013, *A&A*, 553, A56
- Kashlinsky, A., Atrio-Barandela, F., Kocevski, D., & Ebeling, H. 2008, *ApJ Letters*, 686, L49
- Kashlinsky, A., Atrio-Barandela, F., Ebeling, H., Edge, A., & Kocevski, D. 2010, *ApJ Letters*, 712, L81
- Kirshner, R. P., Oemler, A., Jr., Schechter, P. L., & Shethman, S. A. 1987, *ApJ*, 314, 493
- Komatsu E., Smith K. M., Dunkley J., Bennett C. L., Gold B., Hinshaw G., Jarosik N., Larson D., Nolte M. R., Page L., Spergel D. N., Halpern M., Hill R. S., Kogut A., Limon M., Meyer S. S., Odegard N., Tucker G. S., 2011, *ApJS*, 192, 18
- Land, K., & Magueijo, J. 2005, *Physical Review Letters*, 95, 071301
- Lin, H.-N., Wang, S., Chang, Z., & Li, X. 2016, *MNRAS*, 456, 1881
- Marinoni, C., Bel, J., & Buzzi, A. 2012, *JCAP*, 10, 036
- Meegan, C. A., Fishman, G. J., Wilson, R. B., et al. 1992, *Nature*, 355, 143
- Moss, A., Scott, D., Zibin, J. P., & Battye, R. 2011, *Physical Review D*, 84, 023014
- Pandey, B., & Bharadwaj, S. 2005, *MNRAS*, 357, 1068
- Pandey, B. 2013, *MNRAS*, 430, 3376
- Pandey, B. 2016, *MNRAS*, 462, 1630
- Pandey, B. 2016, *MNRAS*, 463, 4239
- Pandey, B. 2017, *MNRAS*, 468, 1953
- Penzias, A. A., & Wilson, R. W. 1965, *ApJ*, 142, 419
- Planck Collaboration, Ade, P. A. R., Aghanim, N., et al. 2014, *A&A*, 571, A23
- Planck Collaboration, Ade, P. A. R., Aghanim, N., et al. 2016, *A&A*, 594, A16
- Planck Collaboration, Ade, P. A. R., Aghanim, N., et al. 2016, *A&A*, 594, A13
- Schwarz, D. J., Starkman, G. D., Huterer, D., & Copi, C. J. 2004, *Physical Review Letters*, 93, 221301

- Schwarz, D. J., & Weinhorst, B. 2007, *A&A*, 474, 717
- Shandarin, S. F., & Zeldovich, Y. B. 1989, *Reviews of Modern Physics*, 61, 185
- Shannon, C. E. 1948, *Bell System Technical Journal*, 27, 379-423, 623-656
- Scharf, C. A., Jahoda, K., Treyer, M., et al. 2000, *ApJ*, 544, 49
- Smoot, G. F., Bennett, C. L., Kogut, A., et al. 1992, *ApJ Letters*, 396, L1
- Strauss, M. A., Weinberg, D. H., Lupton, R. H., et al. 2002, *AJ*, 124, 1810
- Szapudi, I., Kovács, A., Granett, B. R., et al. 2015, *MNRAS*, 450, 288
- Watkins, R., Feldman, H. A., & Hudson, M. J. 2009, *MNRAS*, 392, 743
- Wilson, R. W., & Penzias, A. A. 1967, *Science*, 156, 1100
- Wu, K. K. S., Lahav, O., & Rees, M. J. 1999, *Nature*, 397, 225
- Yoon, M., Huterer, D., Gibelyou, C., Kovács, A., & Szapudi, I. 2014, *MNRAS*, 445, L60
- York, D. G., et al. 2000, *AJ*, 120, 1579
- Zeldovich, Y. B. 1970, *A&A*, 5, 84

**APPENDIX A:**

Table A1: Galactic coordinates of the centers of the regions used for testing the direction dependence of the anisotropy parameter  $a_{lb}$ . These regions correspond to the HEALPix pixels at resolution  $N_{\text{side}}^{\text{region}} = 4$ .

Region	galactic longitude	galactic latitude
1	56.25000	41.81031
2	75.00000	54.34091
3	15.00000	54.34091
4	45.00000	54.34091
5	67.50000	66.44354
6	22.50000	66.44354
7	45.00000	78.28415
8	168.75000	41.81031
9	165.00000	54.34091
10	157.50000	66.44354
11	112.50000	66.44354
12	135.00000	78.28415
13	202.50000	30.00000
14	213.75000	41.81031
15	191.25000	41.81031
16	195.00000	54.34091
17	225.00000	54.34091
18	247.50000	66.44354
19	202.50000	66.44354
20	225.00000	78.28415
21	337.50000	66.44354
22	315.00000	78.28415
23	180.00000	30.00000

This paper has been typeset from a  $\text{\TeX}/\text{\LaTeX}$  file prepared by the author.